Biophysical Journal, Volume *110*

Supplemental Information

Intracellular Pressure Dynamics in Blebbing Cells

Wanda Strychalski and Robert D. Guy

Supporting Material
Intracellular Pressure Dynamics in Blebbing Cells

Wanda Strychalski and Robert D. Guy

S1. Model Details

The membrane and cortex are represented by continuous one-dimensional curves immersed in a two-dimensional fluid domain. The cytoskeleton is represented by a two-dimensional structure immersed in the fluid. Our model is formulated using the immersed boundary (IB) method, where structures are represented in a moving, Lagrangian coordinate system, while fluid variables are located on a fixed, Eulerian coordinate system [1]. A surface force density on on an immersed structure is communicated to the fluid coordinates as follows,

$$\boldsymbol{f} = \mathcal{S}\boldsymbol{F} = \int_\Gamma \boldsymbol{F}(\boldsymbol{s},t)\delta(\boldsymbol{x} - \boldsymbol{X}(\boldsymbol{s},t))\, d\boldsymbol{s}, \tag{S1.1}$$

where $\boldsymbol{s} \in \Gamma$ is the material coordinate and $\boldsymbol{X}(\boldsymbol{s},t)$ denotes the physical position of material point $\boldsymbol{s}$ at time t. The interpolation operator is given by

$$\boldsymbol{U} = \mathcal{S}^*\boldsymbol{u} = \int_\Omega \boldsymbol{u}(\boldsymbol{x},t)\delta(\boldsymbol{x} - \boldsymbol{X}(s,t))d\boldsymbol{x}, \tag{S1.2}$$

where Ω represents the fluid domain.

The Lagrangian drag force density on the cortex due to the fluid is

$$\boldsymbol{F}^{\text{cortex}}_{\text{drag}} = \xi\ (\mathcal{S}^*\boldsymbol{u} - \boldsymbol{U}_{\text{cortex}})\,, \tag{S1.3}$$

where ξ is a drag coefficient inversely proportional to cortical permeability. Similarly, the drag force density on the cytoskeleton is

$$\boldsymbol{F}^{\text{cyto}}_{\text{drag}} = \frac{\mu}{\kappa}\,(\mathcal{S}^*\,\boldsymbol{u} - \boldsymbol{U}_{\text{cyto}})\,, \tag{S1.4}$$

where κ is the permeability of the cytoskeleton.

The Lagrangian elastic force densities on the membrane and cortex are computed by

$$\boldsymbol{F}^{i}_{\text{elastic}} = \frac{\partial}{\partial s}\,(T_i\,\boldsymbol{\tau_i})\,, \tag{S1.5}$$

where T_i is tension and $\boldsymbol{\tau_i}$ is the tangent vector to the curve $\Gamma_i = \boldsymbol{X}_i(s,t)$, $i = $ mem, cortex. In reference arc length coordinates, tension is given by

$$T_i = \gamma_i + k_i\left(\Big|\frac{\partial \boldsymbol{X}_i}{\partial s}\Big| - 1\right), \tag{S1.6}$$

which describes an elastic material with stiffness k_i with an additional resting tension γ_i. Although a pure bilipid membrane is inextensible, the cell membrane surface area can increase as a result of unfurling and extocytosis. For simplicity, we include a stretching term in addition to a surface tension term to take these effects into account and model the membrane as a linearly elastic material.

Membrane-cortex adhesion is modeled by elastic springs attaching the membrane to the cortex with a force density given by

$$\boldsymbol{F}^{\text{mem/cortex}}_{\text{adhesion}} = k_{\text{adh}}\Big(|\boldsymbol{X}_{\text{mem}} - \boldsymbol{X}_{\text{cortex}}|\Big)\frac{\boldsymbol{X}_{\text{mem}} - \boldsymbol{X}_{\text{cortex}}}{|\boldsymbol{X}_{\text{mem}} - \boldsymbol{X}_{\text{cortex}}|}. \tag{S1.7}$$

The adhesion force density on the membrane is the opposite of the corresponding force density on the cortex, with the proper scaling to ensure that the two forces balance,

$$\int_\Omega \mathcal{S}\boldsymbol{F}^{\text{mem/cortex}}_{\text{adhesion}}\, d\boldsymbol{x} + \int_\Omega \mathcal{S}\boldsymbol{F}^{\text{cortex/mem}}_{\text{adhesion}}\, d\boldsymbol{x} = 0. \tag{S1.8}$$

Given the stiffness coefficient $k_{\text{adh}}^{\text{mem/cortex}}$ in Table S1, the corresponding stiffness coefficient for the cortex is obtained by $k_{\text{adh}}^{\text{cortex/mem}} = k_{\text{adh}}^{\text{mem/cortex}} ds_{\text{mem}}/ds_{\text{cortex}}$, where ds_i represents the arc length differential in reference coordinates. Similarly, for cortex-cytoskeleton adhesion, given the parameter $k_{\text{adh}}^{\text{cortex/cyto}}$ in Table S1, we have $k_{\text{adh}}^{\text{cyto/cortex}} = k_{\text{adh}}^{\text{cortex/cyto}} ds_{\text{cortex}}/dA_{\text{cyto}}$, where dA_{cyto} represents the reference area differential of the cytoskeleton.

The cytoskeleton is modeled as a porous neo-Hookean elastic structure. Elastic forces are computed using the energy functional-based version of the IB method proposed in [2]. The elastic properties are characterized by a strain energy $W = W(\mathcal{A})$, where $\mathcal{A} = \partial \boldsymbol{X}/\partial \boldsymbol{s}$ is the network deformation gradient tensor, and $\boldsymbol{X}(\boldsymbol{s}, t)$ is the current location of the cytoskeleton as a function of its Lagrangian coordinate $\boldsymbol{s}$. The strain energy of a neo-Hookean elastic material is

$$W(\mathcal{A}) = \frac{\mu_E}{2}\left(\frac{\text{tr}(\mathcal{A}\mathcal{A}^T)}{J^{2/n}} - n\right) + \frac{G}{2}\left(J-1\right)^2, \tag{S1.9}$$

where μ_E denotes the elastic shear modulus, $G = 2\mu_E/n + \lambda_E$ is the elastic bulk modulus, λ_E is the second Lamé constant, $J = \det \mathcal{A}$ is the determinant of the deformation gradient tensor, and n represents the spatial dimension of the problem. We choose $\lambda_E = \mu_E$ so that $G = 2\mu_E$ in 2D.

The Lagrangian elastic force density is given by the variational derivative of the energy: $\boldsymbol{F}_{\text{elastic}}^{\text{cyto}} = -\delta E/\delta \mathbf{X}$, where E is the total energy of the system $E = \int_\Gamma W d\mathbf{s}$. Our model formulation with this approach for computing elastic forces was shown to match the classical equations of poroelasticity in [3].

The membrane moves with the fluid velocity, and the velocities of the cortex and cytoskeleton are given by Eqs. (7) and (8),

$$\frac{d\boldsymbol{X}_{\text{mem}}}{dt} = \mathcal{S}^* \boldsymbol{u} = \boldsymbol{U}, \tag{S1.10}$$

$$\frac{d\boldsymbol{X}_{\text{cortex}}}{dt} = \boldsymbol{U}_{\text{cortex}} = \frac{1}{\xi}\left(\boldsymbol{F}_{\text{elastic}}^{\text{cortex}} + \boldsymbol{F}_{\text{adhesion}}^{\text{cortex/mem}} + \boldsymbol{F}_{\text{adhesion}}^{\text{cortex/cyto}}\right) + \boldsymbol{U}, \tag{S1.11}$$

$$\frac{d\boldsymbol{X}_{\text{cyto}}}{dt} = \boldsymbol{U}_{\text{cyto}} = \frac{\kappa}{\mu}\left(\boldsymbol{F}_{\text{elastic}}^{\text{cyto}} + \boldsymbol{F}_{\text{adhesion}}^{\text{cyto/cortex}}\right) + \boldsymbol{U}. \tag{S1.12}$$

Discussion of model parameters

In [4] we explored the effects of altering membrane and cortex stiffness. These mechanical parameters primarily affect the shape of the resulting bleb rather than the dynamics of bleb expansion. Increasing (decreasing) membrane stiffness and tension will result in smaller (larger) blebs. Altering membrane stiffness does not significantly affect bleb expansion dynamics, but has a mild effect on the final bleb size, i.e. decreasing membrane stiffness results in slightly larger steady state bleb size. Increasing (decreasing) cortical tension will result in higher (lower) intracellular pressure and larger (smaller) blebs. Decreasing cortical stiffness will result in unphysical bleb shapes.

The stiffness coefficient for adhesion between the membrane and cortex must be sufficiently stiff to obtain a realistic bleb morphology. Decreasing this value will results in a broader (and less circular) bleb because of separation of the cortex and membrane near the edge of the bleb neck. Increasing the value above that used in the model has a negligible effect on bleb morphology. Similarly, the value of the stiffness coefficient for adhesion between the cortex and cytoskeleton was chosen to be large enough so that steady state bleb size was independent of its value.

We follow the analysis in [4] to relate cortical drag in the model to both volume fraction and average pore size of the cortex. In [4], we showed that the permeability (κ) and drag coefficient (ξ) were related by $\kappa = \mu a/\xi$, where a is the thickness of the cortex and μ is the viscosity of the cytosol. Using the values $a = 0.1$ μm, $\mu = 0.01$ Pa·s, and $\xi = 10$ pN/μm^3, the permeability of the cortex is $\kappa = 10^{-4}$ μm^2, which is in line with the values of cytoplasmic permeability explored in the main text. Following [4] and assuming the typical radius of an actin bundle in the cortex is $\lambda = 10$ nm,

Symbol	Quantity	Value
r_{cortex}	Cortex radius	9.99 μm
$k_{\text{adh}}^{\text{mem/cortex}}$	Membrane/cortex adhesion stiffness coefficient	4000 pN/μm^3
$k_{\text{adh}}^{\text{cortex/cyto}}$	Cortex/cytoskeleton adhesion stiffness coefficient	$2.5 \cdot 10^3$ pN/μm^3

Table S1: Additional model parameters.

we estimate that this permeability corresponds to a cortical volume fraction of $\phi = 0.164$ and an average pore size 20.6 nm.

An average pore size of 20.6 nm is in agreement with the low end of estimates of $20 - 200$ nm taken from scanning electron micrographs of the cortex from [5]. If we decreased the value of cortical drag (increased cortical permeability), we would obtain a value for cortical pore size that would better agree with experimental data from [5]. However, we note that using this value of cortical permeability (10^{-4} μm^2) results in a bleb expansion time of less than 1 s in the viscous fluid model of the cytoplasm from [4]. Therefore, decreasing cortical drag would not significantly affect bleb expansion dynamics in the poroelastic model because the forces from cytoplasmic drag and elasticity are the dominant forces that determine bleb expansion dynamics.

S2. Numerical Methods

We use a fractional stepping approach that allows for the fluid and structure updates to proceed sequentially as described in [3]. Given the current position of the structure, the system is advanced in time as follows:

1. Compute elastic forces based on the current membrane, cortex, and cytoskeleton configuration ($\boldsymbol{X}_i^n = \boldsymbol{X}_i(\boldsymbol{s}, t^n)$, where i denotes the structure: membrane, cortex, or cytoskeleton) using the constitutive laws described in Section S1.
2. Spread the force densities onto nearby Eulerian points using Eq. (S1.1).
3. Solve the forced Stokes equations to obtain the fluid velocity $\boldsymbol{u}$.
4. Interpolate the fluid velocity to the structure using Eq. (S1.2) to obtain $\boldsymbol{U}$.
5. Compute the porous structure velocities by Eqs. (7) and (8), and update the structure by

$$\boldsymbol{X}_i^{n+1} = \boldsymbol{X}_i^n + \Delta t \left(\frac{1}{\zeta} \sum \boldsymbol{F}^i + \boldsymbol{U} \right), \tag{S2.1}$$

where ζ indicates the drag coefficient of the cortex or cytoskeleton, and the forces acting on the respective structure denoted by $\sum \boldsymbol{F}^i$ are in Eqs. (7) and (8). The membrane is updated by the fluid velocity.

For the simulations presented in this manuscript, we use periodic boundary conditions on the Eulerian domain and a Fourier-spectral method to solve the Stokes equations.

Because of the large pressure drop across the cell membrane, unphysical spurious velocity is introduced when using standard approximate δ functions, such as Peskin's approximate δ function [6]. Therefore, we construct a more accurate approximation to the δ function directly in Fourier space which results in more accurate solutions. Note that in Fourier space, the operator in Eq. (S1.1) can be written as

$$\widehat{\boldsymbol{f}_{\boldsymbol{k}}} = \int_\Gamma \boldsymbol{F}(\boldsymbol{X}(s)) \exp\left(i\mathbf{k} \cdot \boldsymbol{X}\right) \, ds. \tag{S2.2}$$

Because evaluating the discretized version of this integral is computationally expensive, we use the nonuniform fast Fourier transform (NUFFT) described in [7] to approximate the Fourier transform (FT) of the spread force density. We also use the acceleration techniques described in [7] in our

Symbol	Quantity	Value
L	Fluid computational domain size	30 μm
M	Mesh size	64
Δx	Fluid grid step size	L
Δs	Initial structure grid step size	$\Delta x/2$ (boundary) and Δx (interior)
Δt	Time step size	$1 \cdot 10^{-5} - 7 \cdot 10^{-5}$ s
M_r	Oversampled mesh size for NUFFT	$2M$
M_{sp}	NUFFT spread width	8
τ	NUFFT parameter	$12/M^2$

Table S2: Computational parameters.

algorithms for the spreading and interpolation operators. The computational parameters M_r, M_{sp}, and τ are used in the algorithm described in [7].

Before solving Stokes equation, we filter the forces from Eq. (S2.2) using a second-order raised cosine filter [8],

$$\sigma(k) = \frac{1}{2}\left(1 + \cos\left(\frac{2\pi k}{N}\right)\right). \tag{S2.3}$$

Filtering is necessary to remove the Gibbs phenomenon that would otherwise occur in the pressure field.

Important parameters for the computational methods are listed in Table S2. We used an adaptive mesh to model the cytoskeleton. The unstructured mesh is more refined near the boundary with approximately 2 Lagrangian points per Eulerian grid cell and 1 Lagrangian point per Eulerian grid cell in the interior (Fig. S1). We used `distmesh` to generate the unstructured mesh [9].

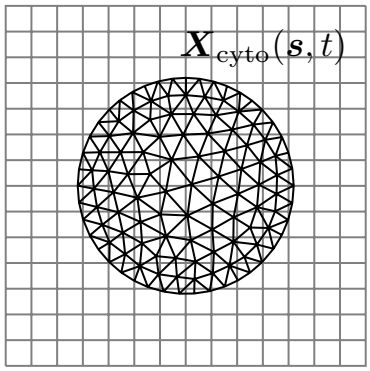

Figure S1: Schematic for the unstructured grid representing the cytoskeleton and the Eulerian grid. The unstructured grid has a spacing of approximately $\Delta x/2$ near the boundary and Δx in the interior.

S3. Dynamics of cytoskeletal compression

The elastic forces of the cytoskeleton are computed from the variation of the total energy as described in Section S1. The term $G/2(J-1)^2$ in the strain energy density function, Eq. (S1.9), accounts for the energy of volumetric change from compression and expansion. Local volume changes can be quantified by the strain $(J-1)$, and they give rise to an isotropic stress of strength $G(J-1)$. During blebbing, the cytoskeleton is compressed ($J < 1$), and one can identify $-G(J-1)$ as a cytoskeletal pressure acting against compressive stresses during bleb expansion.

Figure S2a shows snapshots of this cytoskeletal pressure for the same simulation presented in Fig. 2b in the main text. Shortly after after bleb initiation, a localized compression develops near

the nucleation site, and then on a longer time scale a compression propagates across the cell and approaches a steady state spatial profile. These dynamics of elastic stress are like those of the pressure (shown in Fig. 2b).

At steady state the compression is approximately spatially uniform throughout much of the cell away from the nucleation site. This uniform compression results in a uniform cytoskeleton pressure that relieves intracellular pressure. Figs. S2bc show slices of the cytoskeletal pressure and the intracellular pressure along the middle of the cell, respectively. By $t = 8$ s, at the side of the cell away from the bleb, we see that the pressure has dropped by about 15 Pa, while the cytoskeletal pressure has risen by about 13.5 Pa. Thus most of the pressure dropped is being balanced by the compression of the cytoskeleton. The difference of 1.5 Pa is comparable to the pressure drop we observed in the fluid model; see Fig. 2c in the main text.

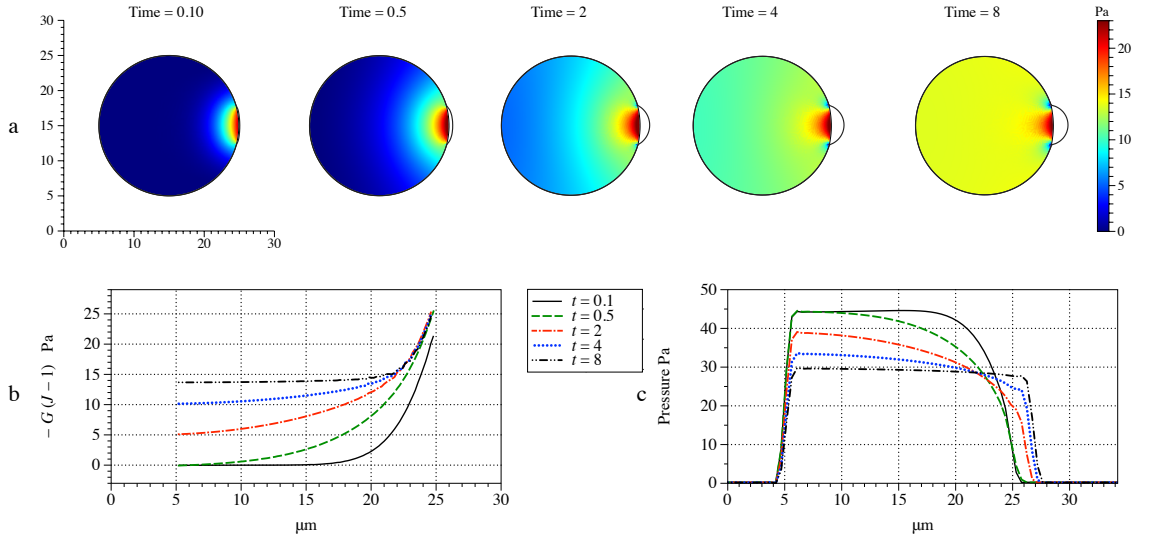

Figure S2: Membrane position and elastic pressure in the cytoskeleton $-G(J-1)$ at several time values in the bleb model (a) when permeability $\kappa = 10^{-3}\,\mu\text{m}^2$ and $G = 500$ Pa. (b) The horizontal elastic pressure profile across the center of the cell (when the vertical axis equals 15 μm in (a)) at several time values and (c) corresponding fluid pressure profiles across the center of the cell.

S4. Two bleb simulations with a fluid cytoplasm

We simulate two bleb experiments where the cytoplasm is modeled as a viscous fluid ($\kappa = \infty$). All parameters are the same as those given for the fluid model of the cytoplasm in the results section. In particular, membrane stiffness was increased to 100 pN/μm to control bleb growth. Following the computational setup for the two-bleb experiments in the results, the second bleb is initiated close to the first bleb (at a 90° angle) and across the cell from the first bleb (at a 180° angle). Figure S3 shows bleb size over time for both two bleb experiments. The first bleb expands, then shrinks as pressure is relieved by the second bleb's initiation and expansion. The first and second bleb size time courses are very similar both configurations.

S5. Reduced model

Consider a cylindrical tube of length L filled with a low-volume-fraction, contractile poroelastic network (see Fig. S4). At the bottom of the tube, the network is attached to an impermeable wall where its velocity and displacement are zero. The top of the tube is free to deform, and its motion is determined by a stress balance at the interface.

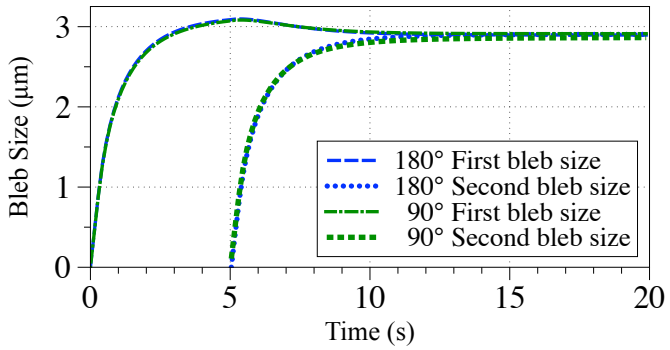

Figure S3: Bleb size over time when the second bleb is initiated 5 seconds after the first one and the cytoplasm is modeled as a viscous fluid. The second bleb is initiated close to the first bleb (at a 90° angle) and across the cell from the first bleb (at a 180° angle)

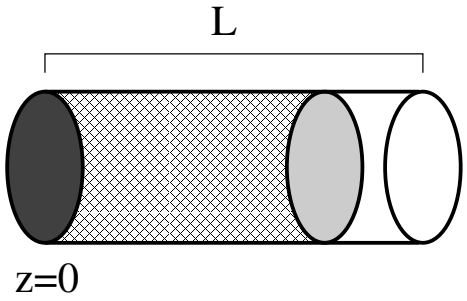

Figure S4: A cylindrical tube of length L filled with a low-volume-fraction, contractile poroelastic network fixed at $z = 0$ and free to move at the other end.

We assume that the deformation is only in the axial direction. Let $q(z,t)$ denote the displacement of the network. We assume small deformation so that the velocity of the network is q_t and the elastic stress is Gq_z, where G is the bulk modulus. Because of incompressibility, the fluid velocity is zero, and so the drag force on the network is simply $-(\mu/\kappa)q_t$. The displacement is zero at the attached boundary ($z = 0$); on the free boundary ($z = L$) the elastic stress is balanced by the contractile stress (σ). We assume that at time zero, the network is experiences no deformation. The system of equations describing this problem is

$$-\frac{\mu}{\kappa}q_t + Gq_{zz} = 0 \tag{S5.1}$$
$$q(0,t) = 0 \tag{S5.2}$$
$$Gq_z(L,t) + \sigma = 0 \tag{S5.3}$$
$$q(z,0) = 0. \tag{S5.4}$$

The steady-state solution is $q^{ss} = -(\sigma/G)z$. At steady-state the network is compressed and the elastic force balances the applied contraction; that is, and total stress (elastic plus contractile) is uniformly zero.

We nondimensionalize the equations by scaling space by the tube size L, displacement by steady-state value at the free end ($L\sigma/G$), and time by the diffusion time scale ($L^2\mu/(G\kappa)$). This gives the parameter-free dimensionless system of equations

$$q_t = q_{zz} \tag{S5.5}$$
$$q(0,t) = 0 \tag{S5.6}$$
$$q_z(1,t) = -1 \tag{S5.7}$$
$$q(z,0) = 0. \tag{S5.8}$$

In dimensionless variables, the diffusion time scale is $t = 1$, which we interpret as the characteristic timescale to approach equilibrium.

The steady-sate solution is $q^{ss}(z) = -z$. Let $q(z,t) = w(z,t) + q^{ss}(z)$, and so w satisfies

$$w_t = w_{zz} \tag{S5.9}$$
$$w(0,t) = 0 \tag{S5.10}$$
$$w_z(1,t) = 0 \tag{S5.11}$$
$$w(z,0) = z. \tag{S5.12}$$

The solution can be written as

$$w(z,t) = \sum_{k=0}^{\infty} A_k \exp\left(-\lambda_k^2 t\right) \sin\left(\lambda_k z\right), \tag{S5.13}$$

where

$$\lambda_k = \frac{\pi(1+2k)}{2}, \tag{S5.14}$$

and

$$A_k = (-1)^k \frac{2}{\lambda_k^2}. \tag{S5.15}$$

In the blebbing model, where the cortex and the membrane are attached, pressure balances the cytoskeletal stresses placed on the membrane. Analogously we examine how the stresses of the free boundary affect the stresses on the attached boundary in response to the displacement on the free boundary. The stress applied to the wall at $z = 0$ is $F_{\text{wall}} = q_z(0,t) + 1 = w_z(0,t)$. This function is plotted in Fig. S5 (left). By time 1 (the diffusive time scale), the wall stress has dropped by almost 90% of its initial value. Figure S5 (right) shows the relative change of the wall stress over the first 0.1 time units. What is very interesting to note is that by time 0.1, the wall force has dropped by about 5%. This means that, on a time scale which is an order of magnitude shorter than the diffusive time scale, there is a significant change in stress on the opposite side of the tube.

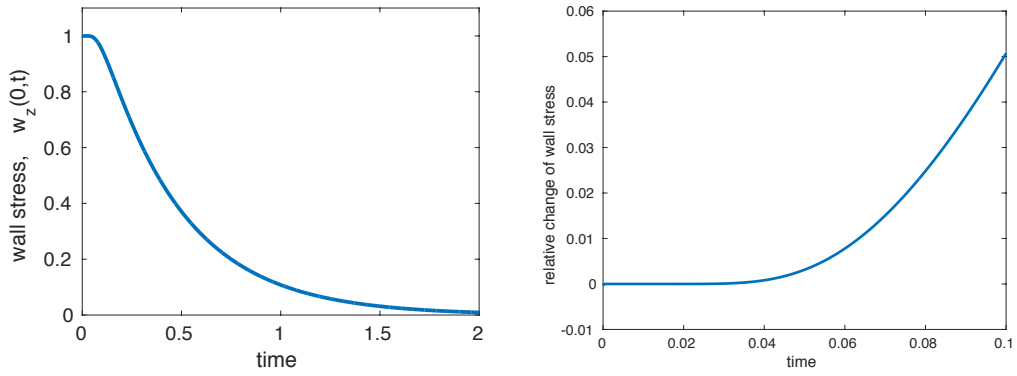

Figure S5: Left: Stress on the stationary wall over time. Right: Relative change of the wall stress over the first 0.1 of time.

Supporting References

[1] C. S. Peskin, Numerical analysis of blood flow in the heart, J. Comput. Phys. 25 (3) (1977) 220–252.

[2] D. Devendran, C. S. Peskin, An immersed boundary energy-based method for incompressible viscoelasticity, J. Comput. Phys. 231 (14) (2012) 4613 – 4642.

[3] W. Strychalski, C. A. Copos, O. L. Lewis, R. D. Guy, A poroelastic immersed boundary method with applications to cell biology, J. Comput. Phys. 282 (0) (2015) 77 – 97.

[4] W. Strychalski, R. D. Guy, A computational model of bleb formation, Math. Med. Biol. 30 (2) (2013) 115–130.

[5] G. T. Charras, C. K. Hu, M. Coughlin, T. J. Mitchison, Reassembly of contractile actin cortex in cell blebs, J. Cell. Biol. 175 (3) (2006) 477–90. doi:10.1083/jcb.200602085.

[6] C. S. Peskin, The immersed boundary method, Acta Numer. 11 (2002) 479–517.

[7] L. Greengard, J.-Y. Lee, Accelerating the nonuniform fast fourier transform, SIAM Rev. 46 (3) (2004) 443–454.

[8] R. Peyret, Spectral Methods for Incompressible Viscous Flow, Springer, New York, 2002.

[9] P. Persson, G. Strang, A simple mesh generator in matlab, SIAM Rev. 46 (2) (2004) 329–345.